Si decline and diatom evolution: Insights from physiological experiments

Alessandra Petrucciani[1], Andrew H. Knoll[2]
and Alessandra Norici[1,3]*

[1]Laboratory of Algal and Plant Physiology, Dipartimento di Scienze della Vita e dell'Ambiente,
Università Politecnica delle Marche, Ancona, Italy, [2]Department of Organismic and Evolutionary
Biology, Harvard University, Cambridge, MA, United States, [3]Faculty of Sciences, Shantou
University-Università Politecnica delle Marche (STU-UNIVPM) Joint Algal Research Center, Shantou
University, Shantou, China

In today's oceans, diatoms are abundant and diverse primary producers distinguished by their silica shells. Although molecular clocks suggest that diatoms arose as much as 250 million years ago (Ma), the earliest known diatom fossils date from 190 Ma, leading to the suggestion that early diatoms were at best lightly silicified. By the Cretaceous Period, large circular (in cross section) diatoms with highly silicified frustules thrived in surface oceans, only later to be joined by species with elongated and thinner frustules, as well as lower SiO_2 content. Decreased Si availability in surface oceans has been proposed as a principal driver of diatom evolution. Here, we investigate this through physiological experiments assessing the functional acclimation response of diatoms to reconstructed paleo-seawater. Four diatom species, differing in size and shape, were acclimated to reconstructed paleoenvironments mimicking Mesozoic/Cenozoic concentrations of nutrients in the presence of different Si regimes. When exposed to 500 µM Si, all populations, save for that of *Conticribra weissflogii*, became more highly silicified; the higher Si content per cell at 500 µM Si coincided with slower growth in small-sized cells. All species except *C. weissflogii* also showed lower photosynthetic efficiency as well as greater cell volume in comparison with diatoms acclimated to 205 or 25 µM Si. Average cell stoichiometry correlates with cell shape, but not size; pennates, in particular *Phaeodactylum tricornutum*, showed an acclimatory response to Si regimes, modulating Si use efficiency (the lower the external Si concentrations, the higher the C and N quotas per Si).

Experimental data suggest that in the densely silicified and bigger *C. weissflogii* grown at higher Si, diffusion of silicic acid across membranes made a larger contribution to Si uptake, saving energy which could be reallocated into growth. In contrast, for less highly silicified and smaller species, high energy costs of Si homeostasis needed to prevent the overaccumulation of

intracellular Si limited growth. While our experimental species reacted individualistically to changing silica availability, with distinct levels of plasticity, selective pressure associated with the temporal decline in Si availability may well have favored elongated shapes. Modern, less silicified species are unable to exploit high Si concentrations.

Introduction

In the modern ocean, diatoms are abundant and diverse primary producers, distinguished by their silica shells, or frustules. Accounting for some 20% of primary production on Earth, diatoms sustain the global food web while being responsible for 240 Tmol of biogenic silica precipitation annually (Loucaides et al., 2012; Vallina et al., 2014; Malviya et al., 2016; Sutton et al., 2018; Vincent and Bowler, 2020; Tréguer et al., 2021). The oldest known diatom fossils occurred in Late Jurassic (ca. 165 million years old, Ma) amber (Girard et al., 2020), and since that time, diatoms have diversified to play a crucial role in ocean ecology (Armbrust, 2009); indeed, their radiation has molded marine ecosystems through time (Finkel and Kotrc, 2010; Kotrc and Knoll, 2015; Cermeño et al., 2015; Medlin, 2015; Knoll and Follows, 2016; Benoiston et al., 2017), affecting both the carbon and silica cycles (Siever, 1992; Ragueneau et al., 2006; Renaudie, 2016; Conley et al., 2017; Tréguer et al., 2018).

In Precambrian oceans, before the evolution of organisms with biomineralized skeletons, the concentration of dissolved silica (DSi) in seawater must have been much higher than today (Siever, 1992; Conley and Carey, 2015; Conley et al., 2017). The Ediacaran/Cambrian radiations of siliceous sponges and radiolarians established biology as a major component of the silica cycle, demonstrably changing the depositional dynamics of silica in the oceans (Maliva et al., 1989; Kidder and Tomescu, 2016) and probably decreasing the seawater DSi concentration (Conley et al., 2017). New biological influences emerged during the Mesozoic Era, as multiple clades of silica biomineralizing protists spread through the oceans (Kotrc and Knoll, 2015; Marron et al., 2016). Diatoms, in particular, are thought to have further drawn down DSi in surface seawater, leading to the low concentration (<30 μM) observed today (Racki and Cordey, 2000; Conley et al., 2017). Changes in hydrothermal fluxes and continental weathering can also have influenced DSi through time (Frings et al., 2016; Conley et al., 2017), but independent perspectives on orogenesis and seafloor spreading suggest that the Mesozoic-Cenozoic DSi decline was largely mediated by biology.

Within diatoms, the diversification of specialized transporters (silicon transporters, SIT) helped to make them the dominant marine DSi utilizers in Cenozoic oceans (Durkin et al., 2016; Fontorbe et al., 2017). As a consequence, competitors for this resource, principally radiolarians and sponges, show declines in test mass and/or environmental distribution (Harper and Knoll, 1975; Maldonado et al., 1999; Lazarus et al., 2009; Hendry et al., 2018). Diatoms themselves show a change in skeletal morphology through time, with a trend toward smaller, more elongated, and less highly silicified frustules toward the present (Finkel et al., 2005; Armbrust, 2009; Finkel and Kotrc, 2010). It is worth noting that factors other than DSi availability may have influenced the evolution of silicifiers (e.g., Finkel et al., 2005; Hendry et al., 2018) and that changing selectivity of preservation may also influence the observed record (Westacott et al., 2021). That noted, could changes in DSi availability have influenced the observed shifts in the fossil record? We hypothesize that decreasing DSi favored smaller and less silicified diatom cells in marine environments. To test this hypothesis, four morphologically distinct modern diatoms (*Chaetoceros muelleri*, *Conticribra weissflogii*, *Phaeodactylum tricornutum*, *Cylindrotheca fusiformis*) were acclimated to paleo-reconstructed environments according to Ratti et al. (2011), modified to mimic Mesozoic to modern changes in DSi concentration. As nutrient limitation is known to affect silica deposition and dissolution in diatoms (Takeda, 1998; Hutchins and Bruland, 1998; Boyle, 1998; De La Rocha et al., 2000; Mosseri et al., 2008; Finkel et al., 2010; Bucciarelli et al., 2010; Cohen et al., 2017; Meyerink et al., 2017; Panagiotopoulos et al., 2020), experiments using reconstructed seawater that include interpreted variation in the bioavailability of N, Fe, Zn, and Mo (Ratti et al., 2011; Giordano et al., 2018) better approximate ancient marine environments and their interactions with organisms. Growth, photosynthetic efficiency, organic and inorganic composition, and frustule morphology were assessed.

Material and methods

Algal cultures

Two centric diatom species, *Chaetoceros muelleri* (CCAP 1010/3, https://www.ccap.ac.uk/) and *Conticribra weissflogii* (*Thalassiosira weissflogii* in earlier literature; DCG 0320, https://bccm.belspo.be/about-us/bccm-dcg), and two raphid pennate diatoms characterized by thin frustules, *Cylindrotheca fusiformis* (NEPCC417) and *Phaeodactylum tricornutum* (DCG 0981), were acclimated for at least 10 generations to three newly designed growth media combining the Mesozoic/Cenozoic concentration of nutrients (as already published by Ratti et al., 2011; Table 1) and the presence of different Si regimes (Table 2) in AMCONA medium (Fanesi et al., 2014) buffered with 10 mM Tris–HCl, pH 8.0.

There are varying estimates for DSi levels in ancient oceans. Siever (1992) proposed that diatom evolution gradually reduced seawater DSi from some 1000 μM to its present level of<30 μM in most surface waters. In contrast, Conley et al. (2017) estimated that DSi concentrations of 500 μM in pre-diatom oceans fell rapidly to near-modern levels as diatoms began their radiation. Most recently, Trower et al. (2021) used Si isotope ratios to argue that DSi levels could have been as low as 150 μM in Paleozoic oceans. Regardless of the starting point, all conclude that diatom radiation reduced DSi concentrations in surface seawater. The DSi values used in our experiments were chosen to explore this range of estimated changes through time.

Acclimated batch cultures were established in 500ml flasks filled with 200 ml of medium and maintained in a culture chamber at 18°C, illuminated with cool white fluorescent lamps at 60 μmol m^{-2} s^{-1} and 12:12-h light–dark cycles. All experiments were carried out in the exponential growth phase.

Specific growth rate and cell volume

Cell number was measured using a CASY TT Cell Counter (Innovatis AG, Reutlingen, Germany). Aliquots of 100 μl of culture were diluted in 10 ml of an electrolyte solution (CASY TON; Innovatis AG). Cells were pumped into the cell counter through a 150μm capillary at a constant flow, and the number of cells was determined through the enumeration of events measured as change in conductivity. The same instrument was

TABLE 1 Mesozoic/Cenozoic concentration of nutrients. Ratti et al., 2011.

Nutrient	Final concentration
NaNO3	10 μM
FeCl$_3$· 6H$_2$O	50 nM
ZnSO$_4$· 7H$_2$O	100 nM
Na$_2$MoO$_4$· 2H$_2$O	105 nM

TABLE 2 Silicic acid concentrations added to the Mesozoic/Cenozoic medium to mimic the progressive DSi depletion through geologic time.

Treatment	Si concentration
Pre- to early diatoms	500 μM
Intermediate	205 μM
Modern	25 μM

also used to measure the cellular size as the volume of electrolyte solution displaced by the passage of cells through a measuring pore (Palmucci et al., 2011). All determinations were carried out on samples from three distinct cultures. Specific growth rates, μ (1), were derived from daily counts of exponentially growing cells, carried out on a minimum of three distinct cultures for each treatment.

$$\mu = \frac{ln(N_t/N_0)}{t} \quad \text{Monod, J. (1949)} \quad (1)$$

where t is time (d), N_0 is the initial cell density (cell· ml^{-1}) at time 0, and N_t is the cell density at the considered time t.

Pigment quantification and photosynthetic efficiency

Algae were centrifuged at 1500 g for 5 min. Then, pigments were extracted from the pellet in 2 ml of 100% (v/v) methanol (Ritchie, 2006); the extracts were stored in the dark, at -20°C overnight. The colorless pellet was then separated from the supernatant by centrifugation at 13,000 g for 5 min. The absorbance of the supernatant was evaluated spectrophotometrically (Beckman DU 640 Spectrophotometer, Beckman Coulter) in a range from 750 to 350 nm (scan speed 0.5 nm). The absorbance (Abs) at wavelengths of 664, 630, and 470 nm was used for pigment quantification of chlorophyll *a*, chlorophyll $c_1 + c_2$, and carotenoids, respectively. Methanol absorbance was used as blank, and absorbance at 730 nm was subtracted to all measurements.

Chlorophyll (Chl) concentrations were calculated according to Ritchie, 2006 equations:

$$\text{Chl } a \left(\mu g \, ml^{-1} \right) = 13.2654 \cdot Abs_{664nm} - 2.6839 \cdot Abs_{630nm} \quad (2)$$

$$\text{Chl } C_1 + C_2 \left(\mu g \, ml^{-1} \right) = 28.8191 \cdot Abs_{630nm} - 6.0138 \cdot Abs_{630nm} \quad (3)$$

$$Total \text{ Chl} \left(\mu g \cdot mL^{-1} \right) = \text{Chl } a + \text{Chl } C_1 + C_2 \quad (4)$$

Carotenoids' concentrations were calculated according to Wellburn, 1994 equations:

$$Total\ carotenoids\ \left(\mu g \cdot ml^{-1}\right)$$

$$= \left(1000 \cdot Abs_{470nm} - 1.63 \cdot Chla - 104.96 \cdot Ch\,C_1 + C_2\right)/221 \tag{5}$$

All results were expressed as pg of pigment per cell (Figure S2).

In vivo variable fluorescence of photosystem II (PSII) chlorophyll *a* (P_{680}) was analyzed using a Dual Pulse Amplitude Modulation (PAM) 100 fluorimeter (Heinz Walz GmbH, Effeltrich, Germany). Samples of 10^7 cells were collected by centrifugation at 1500 g for 5 min, resuspended in 2 ml of fresh growth medium, and dark-adapted for 10 min. Subsequently, samples were transferred into a glass cuvette for the PAM analysis under continuous stirring. The measuring light (40 μmol photons m^{-2} s^{-1}) was turned on to determine the F_0 value, the minimum value for chlorophyll fluorescence. Then, a saturation pulse (10,000 μmol photons m^{-2} s^{-1}, 600 ms) was applied to saturate all centers and allowed to measure the F_m value, the maximum value of fluorescence. The maximum quantum efficiency of PSII, F_v/F_m, was then calculated as follows:

$$\frac{F_V}{F_m} = \frac{(F_m - F_0)}{F_m} \tag{6}$$

F_v/F_m represents a robust indicator of the maximum quantum yield of PSII photochemistry (Misra et al., 2012). All parameters were obtained using the Dual PAM v1.8 software (Walz GmbH, Effeltrich, Germany).

Elemental composition

Cellular C and N contents were determined using an elemental analyzer (ECS 4010, Costech Italy) from 0.1 to 1 mg of dry cells washed twice with an ammonium formate solution isosmotic to the culturing media and dried at 80°C (Giordano et al., 2018). Sulfanilamide (C:N:S = 6:2:1) was used in a standard curve for quantification (Giordano et al., 2018). Data acquisition and analysis were performed with the software EAS Clarity (Costech Analytical Technologies Inc., Milano, Italy; organic composition). All measurements were carried out on three biological replicas.

Similarly prepared samples (0.5–1 mg of dry weight) were analyzed by an elemental analyzer (ECS 4010, Costech Italy) connected to the ID Micro EA isotope ratio mass spectrometer (Compact Science Systems, Lymedale Business Centre, Newcastle-Under-Lyme, United Kingdom) to obtain carbon and nitrogen stable isotope ($\delta^{13}C$ and $\delta^{15}N$) ratios. Urea was the isotopic standard reference showing $\delta^{13}C$ = −36.6‰ and $\delta^{15}N$ = -2.2‰; its replicates were used to normalize isotopic values of algal biomass. Two blank samples (empty aluminum capsules) were analyzed at the start of each analysis to verify that the CO_2 and N_2 backgrounds were low, and urea standards were

also analyzed after every six samples to monitor instrument performance. Data acquisition and analysis were performed with the software EA IsoDelta (Compact Science Systems, Lymedale Business Centre, Newcastle-Under-Lyme, United Kingdom). All the measurements were carried out on three biological replicas.

The absolute abundance of silicon and elements other than C and N was measured using a total reflection X-ray fluorescence spectrometer (S2 PICOFOX, Bruker AXS Microanalysis GmbH, Berlin, Germany) according to Giordano et al. (2018). Sampled diatoms were washed twice with an ammonium formate solution isosmotic to the culturing media and resuspended in 250 μl of dH$_2$O. A solution of 0.1 g l^{-1} Ga (Sigma-Aldrich, St. Luis, MO, USA) in 5% HNO$_3$ was added as internal standard to a final concentration of 0.5 μl l^{-1}. The suspension was carefully vortexed, and an aliquot of 10 μl was deposed on a plastic sample holder, dried on a heating plate, and measured for 1,000 s. Spectral deconvolution and quantification of elemental abundances were performed by the Spectra 6.1 software (Bruker AXS Microanalysis GmbH, Berlin, Germany).

Organic composition

Diatoms collected during the exponential phase were washed twice with a 0.5M solution of ammonium formate and used to prepare samples for analysis of FTIR spectroscopy. Aliquots of 50 μl of cell suspension were transferred to a silicon window and dried at 80°C (Domenighini and Giordano, 2009). FTIR spectra on whole cells were acquired with a Tensor 27 FTIR spectrometer (Bruker Optics, Ettlingen, Germany). Bands were assigned to cellular pools as described by Giordano et al. (2001), and the relative abundances of lipids, carbohydrates, proteins, and silica were calculated *via* band integrals of deconvolved spectra, with OPUS 6.5 software (Bruker Optics GmbH, Ettlingen, Germany). Considering that silica absorbance (∼1,075 cm^{-1}) masks some of the typical carbohydrate bands in diatoms, only the integrated value at ∼1,150 cm^{-1} was used as proxy for carbohydrates (Palmucci et al., 2011). Semiquantification of carbohydrates and lipids was obtained by comparing the total protein content measured by a quantitative method (see below) with the FTIR absorbance ratio between the pool of interest and that of proteins according to Palmucci et al. (2011); the three macromolecular pools expressed in arbitrary units were normalized to the corresponding 500 μM of Si pool.

Protein content was measured according to the Lowry method described by Peterson (1977) on diatoms collected by centrifugation (13,000 g for 5 min) during the exponential phase. A volume of 500 μl 1% sodium dodecyl sulfate (SDS) and 0.1 mol l^{-1} of NaOH were added to the pellet to facilitate membrane disruption and solubilization of proteins. The tubes were vortexed and then incubated at room temperature for 10 min. A volume of 500 μl of reagent A (25% H$_2$O, 25% SDS 10%, 25%

NaOH 0.8M, 25% CTC reagent) was added, and the samples were vortexed and let to sit at room temperature for 10 min. A volume of 250 μl of reagent B (83.3% H_2O, 16.7% Folin and Cicalteau's phenol reagent) was then added, and samples were immediately vortexed vigorously; finally, they were incubated in the dark for 30 min. Afterward, the sample absorbance was measured in a Beckman DU 640 Spectrophotometer (Beckman Coulter) at 750 nm. Protein contents were calculated by interpolating absorbance data in a standard curve constructed with known concentrations of bovine serum albumin (BSA). All the measurements were carried out on three biological replicas, and results were expressed as pg of proteins per cell (Figure S4).

Frustule characterization through scanning electron microscopy

Diatom frustules were obtained through oxidation of the organic material using hydrogen peroxide, H_2O_2. Salts of the culture medium were washed out from the cells for three times with deionized water, then 30% H_2O_2 was added to the cell suspension to a final concentration of about 15%. Samples were dried in oven at 60°C for 1 day (less silicified species, *P. tricornutum* and *C. fusiformis*) or three days (more silicified species, *C. muelleri* and *C. weissflogii*). Finally, the material was washed four times with deionized water to carefully remove H_2O_2. Drops of cleaned material were then poured on a cellulose acetate and cellulose nitrate mixture filter (MF-Millipore™, mesh size 0,45 μm) fixed on conductive carbon adhesive discs pasted on the stub and left to dry completely at 50°C. The stub was then sputter-coated with a thin layer of gold–palladium in a Balzer Union evaporator and analyzed by SEM (High Resolution ZEISS – SUPRA 40). Images were obtained at different magnifications to make morphometric measurements of frustule details (raphe and fibulae in *C. fusiformis*, Reimann et al., 1965; setae and punctae in *C. muelleri*, Reinke, 1984) from at least 10 frustules per each of the three biological replicas.

Statistical analysis

Significant differences among the means of dependent variables in different paleoenvironments (independent variable) were tested with a one-way analysis of variance (ANOVA), followed by Tukey's *post-hoc* test. Macromolecular pools as dependent variables in response to paleoenvironments and according to diatom species (independent variables) were analyzed by two-way ANOVA, followed by Tukey's *post-hoc* test. Comparison of treatment pairs (morphological parameters at 500 and 25 μM Si, Table S2) was achieved with a two-tailed *t*-test. The level of significance was set at 0.05. GraphPad Prism 8.0.2.263 was used to carry out the tests (GraphPad Software, San Diego, CA, USA).

Results

Growth, cell volume, and photosynthetic efficiency

The four diatom populations were acclimated to reconstructed paleoenvironments. Growth of the smaller species *C. muelleri* and *P. tricornutum* was deeply affected by Si availability in the medium (Figure S1); specifically, the higher the DSi concentration, the lower the growth rate (Table 3). In fact, *C. muelleri* cells grew very slowly when DSi was 500 μM. The decrease in growth rate of these species was accompanied by an increase in cell volume (Table 3). Growth rates of the larger species *C. weissflogii* and *C. fusiformis* were similar among the three DSi treatments. High concentrations of silicic acid

TABLE 3 Average ± SD of specific growth rate (μ), cell volume, and *Fv/Fm* in the four diatoms acclimated to different paleoenvironments (n ≥ 3).

		500 μM Si	205 μM Si	25 μM Si
	C. muelleri	0.13 ± 0.04^a	0.48 ± 0.08^b	0.54 ± 0.08^b
Specific growth rate (μ, day^{-1})	*C. weissflogii*	0.28 ± 0.03	0.28 ± 0.01	0.25 ± 0.03
	P. tricornutum	0.29 ± 0.01^a	0.36 ± 0.02^a	0.58 ± 0.04^b
	C. fusiformis	0.41 ± 0.09	0.52 ± 0.05	0.47 ± 0.15
	C. muelleri	581 ± 93^a	470 ± 55^{ab}	439 ± 56^b
Cell volume (μm^3)	*C. weissflogii*	1352 ± 229^a	1713 ± 209^b	1459 ± 160^{ab}
	P. tricornutum	266 ± 50^a	143 ± 20^b	134 ± 50^b
	C. fusiformis	474 ± 64^a	363 ± 28^b	381 ± 75^b
	C. muelleri	0.10 ± 0.05^a	0.41 ± 0.06^b	0.45 ± 0.08^b
Fv/Fm	*C. weissflogii*	0.61 ± 0.14	0.72 ± 0.02	0.74 ± 0.03
	P. tricornutum	0.49 ± 0.04^a	0.67 ± 0.03^b	0.66 ± 0.02^b
	C. fusiformis	0.25 ± 0.05^a	0.60 ± 0.03^b	0.65 ± 0.01^b

Different letters indicate significant differences among conditions in the same species (p > 0.05, one-way ANOVA followed by Tukey's *post-hoc* test, results in Table S3).

mimicking a pre-diatom regime resulted in a lower maximum PSII Quantum Yield in dark-adapted cells, F_v/F_m, of *C. muelleri*, *P. tricornutum*, and *C. fusiformis*. In contrast, *C. weissflogii* did not show any change in photosynthetic efficiency (Table 3).

Elemental composition

When cells were subjected to different Si regimes during growth, all diatoms grown in the highest DSi condition except for *C. weissflogii* accumulated more Si per volume unit (Figure 1). The largest variation was observed in pennate diatoms, *C. fusiformis* and *P. tricornutum*, showing twice the content when the concentration of external silicic acid reached 500 µM as compared to contents in the other conditions. The same was true when the Si content was expressed on a per cell basis (Table S1).

The P cell quota had a similar trend to that of the Si cell quota (Table S1). Only *P. tricornutum* also showed significantly higher C, N, and Fe contents in the highest DSi condition (Table S1). In general, the C:N:P:S:Si ratio of the cells was inversely related to the concentration of silicic acid in the growth medium: lower amounts of assimilated C, N, P, and S per unit of cell Si with higher DSi availability (Table 4). Furthermore, the P cell quota increased with increasing DSi availability (Table S1). Only *P. tricornutum* also showed significantly higher C, N, and Fe contents in the highest DSi condition (Table S1), with the Fe : Si ratio remaining approximately constant across the different Si treatments (Table 4).

Interestingly, our centric and pennate diatoms show divergent trends in carbon isotopic fractionation across treatments (Figure 2).

Centric diatoms significantly increased observed fractionation (more negative $\delta^{13}C$) as DSi decreased, just the opposite of observed trends in our pennate species. Also, a strong correlation (Pearson r = -0.99 in *P. tricornutum* and -0.96 in *C. fusiformis*, Figure S3) between the $\delta^{13}C$ and intracellular Si content was observed in pennate cells, but not in our centric species.

Organic composition

In cells of *C. muelleri*, *C. fusiformis*, and *P. tricornutum*, proteins were more abundant in response to higher silicic acid concentrations in the growth medium (Figure 3 and Figure S4). In pennate diatoms, the same trend was observed for the carbohydrate pool. Save for *C. weissflogii*, all diatoms did not significantly change the lipid pool in response to DSi treatment. Regarding macromolecular ratios, the cellular carbohydrate/lipid ratio showed C reallocation in all species (Table 5). In centric diatoms, the protein-to-carbohydrate ratio was not affected while the protein-to-lipid ratio was significantly higher in response to higher DSi availability (Table 5).

Frustule characterization through scanning electron microscopy

Frustule structure shows only limited variation as a function of treatment. In *C. muelleri*, setae were thicker when grown at high DSi, but not significantly (Figures 4C, D; Table S2). Neither
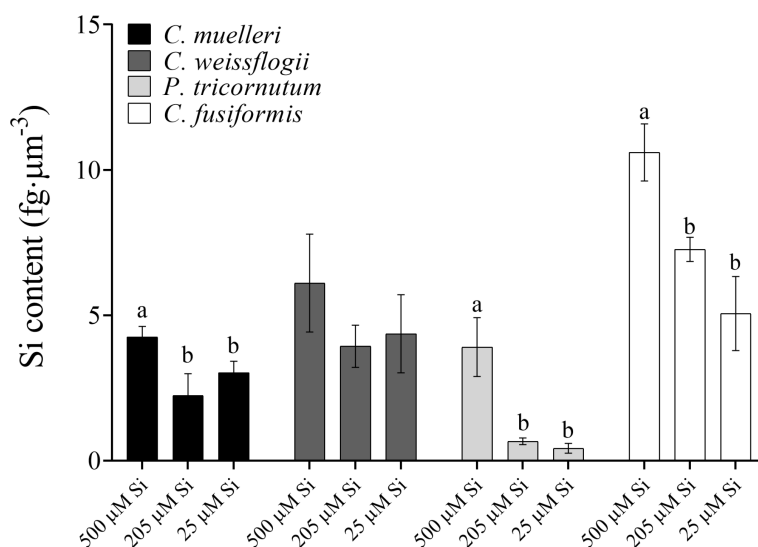
FIGURE 1
Si content per volume (fg·µm^{-3}) in the four diatoms acclimated to different paleoenvironments. Data are means of three biological replicas. Error bars show SD. Different letters represent significant differences among conditions in the same species (p < 0.05, one-way ANOVA followed by Tukey's *post-hoc* test, results in Table S3).

TABLE 4 Cell stoichiometry in relation to Si content (pg·cell^{-1}) of the four diatoms acclimated to different paleoenvironments.
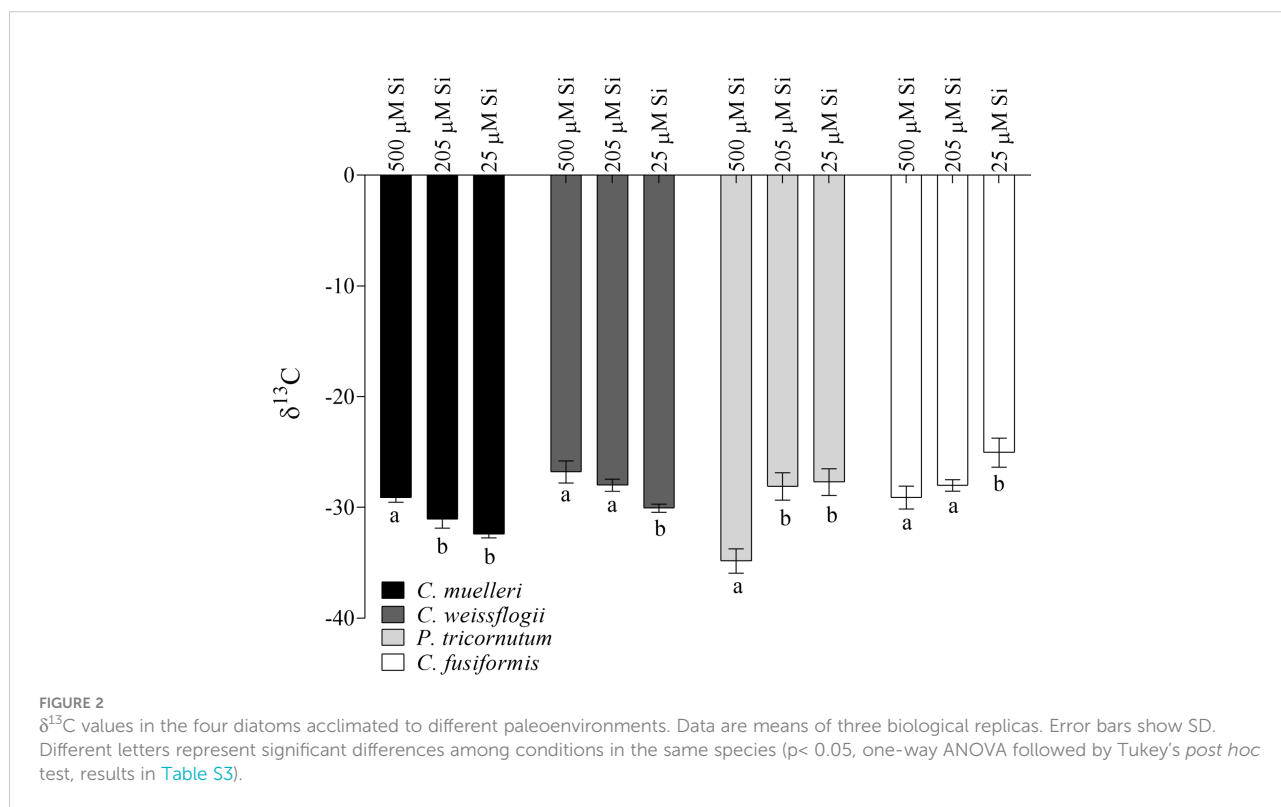
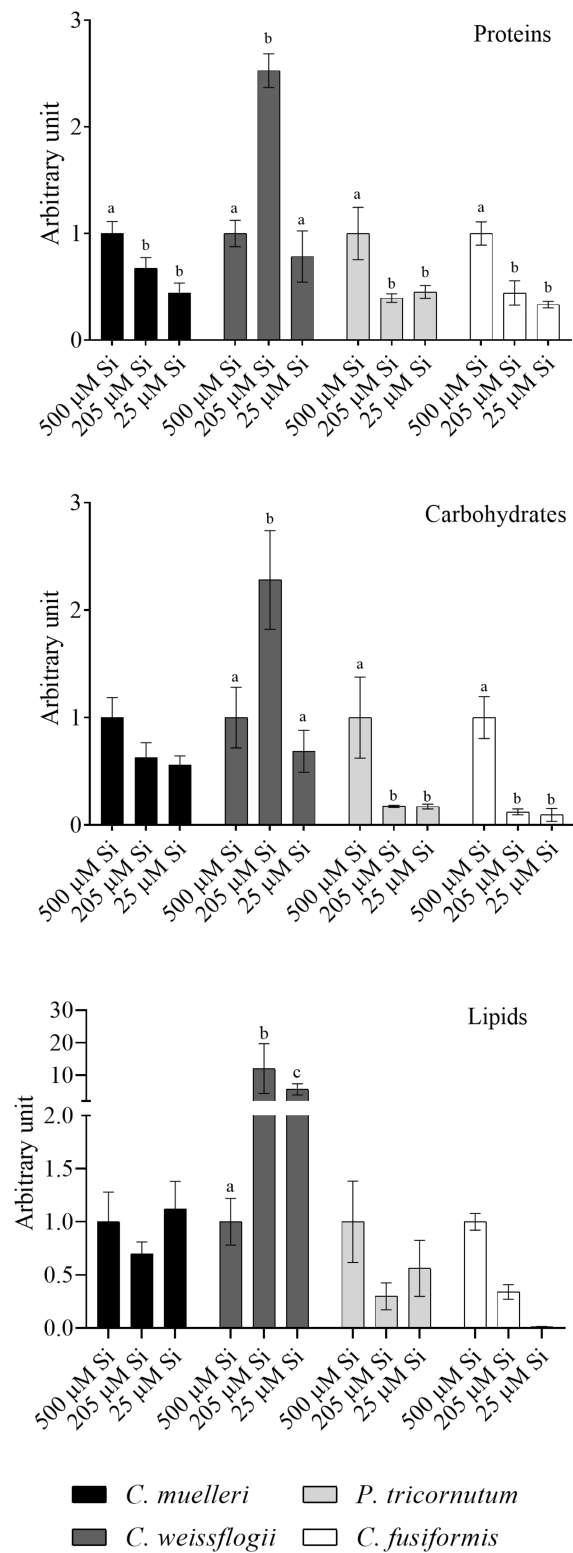|		C : Si	N : Si	P : Si	S : Si	Fe : Si
	500 µM Si	13.56 ± 3.14	2.66 ± 0.97	0.58 ± 0.03	0.18 ± 0.07	0.018 ± 0.007
C. muelleri	205 µM Si	11.23 ± 1.90	2.44 ± 0.39	0.47 ± 0.13	0.33 ± 0.09	0.144 ± 0.099
	25 µM Si	16.13 ± 6.65	3.30 ± 1.52	0.28 ± 0.17	0.26 ± 0.07	0.022 ± 0.002
	500 µM Si	2.38 ± 1.90	0.58 ± 0.57	0.013 ± 0.002	0.04 ± 0.01	0.001 ± 0.001
C. weissflogii	205 µM Si	1.22 ± 0.38	0.19 ± 0.08	0.021 ± 0.001	0.06 ± 0.02	0.006 ± 0.002
	25 µM Si	1.60 ± 0.84	0.19 ± 0.09	0.012 ± 0.007	0.10 ± 0.09	0.004 ± 0.001
	500 µM Si	20.90 ± 7.26[a]	4.34 ± 0.54[a]	0.50 ± 0.07[a]	0.42 ± 0.06[a]	0.083 ± 0.006
P. tricornutum	205 µM Si	78.01 ± 31.42[b]	11.94 ± 4.36[b]	2.67 ± 0.53[b]	3.01 ± 0.42[b]	0.078 ± 0.013
	25 µM Si	93.77 ± 14.44[b]	12.93 ± 2.19[b]	3.47 ± 0.62[b]	4.27 ± 0.73[c]	0.076 ± 0.006
	500 µM Si	3.57 ± 1.60[a]	0.68 ± 0.29[a]	0.16 ± 0.02	0.11 ± 0.08	0.034 ± 0.009[ab]
C. fusiformis	205 µM Si	9.13 ± 1.09[b]	1.74 ± 0.23[b]	0.15 ± 0.01	0.11 ± 0.01	0.005 ± 0.001[a]
	25 µM Si	5.29 ± 1.66[ab]	0.66 ± 0.16[ab]	0.15 ± 0.03	0.35 ± 0.29	0.016 ± 0.009[b]

Data are means of three replicates ± SD. Different letters indicate significant differences among conditions in the same species (p > 0.05, one-way ANOVA followed by Tukey's *post-hoc* test, results in Table S3).

did *C. weissflogii* show any significant difference in frustule morphology as a function of treatment (Figure 4B). By contrast, the pennate species both showed a significant difference between frustules grown at high versus low DSi (Figure 5 and Table S2). Under high DSi, *P. tricornutum* frustules were significantly wider and raphes significantly thicker (Figures 5A, C, D), while the raphe in *C. fusiformis* was significantly wider (Figures 5B, E, F and Table S2).

Discussion

Paleontological and geochemical data support the hypothesis that diatom radiation drove a decline in the DSi of surface seawater that influenced the subsequent evolution of both diatoms and other organisms that form skeletons of silica (Finkel et al., 2005; Rabosky and Sorhannus, 2009; Conley et al., 2017; Hendry et al., 2018). At the same time, other factors, including climate change, orogenesis, and

FIGURE 2
δ^{13}C values in the four diatoms acclimated to different paleoenvironments. Data are means of three biological replicas. Error bars show SD. Different letters represent significant differences among conditions in the same species (p< 0.05, one-way ANOVA followed by Tukey's *post hoc* test, results in Table S3).

FIGURE 3
Protein, carbohydrates, and lipid pools in the four diatoms acclimated to different paleoenvironments. Data are means of three replicates. Error bars show SD. Different letters represent significant differences among conditions in the same species ($p < 0.05$, two-way ANOVA followed by Tukey's *post-hoc* test, results in **Table S3**).

TABLE 5   Macromolecular pool ratios (arbitrary unit) for the four diatoms acclimated to different paleoenvironments.

		500 μM Si	205 μM Si	25 μM Si
Proteins/carbohydrates	C. muelleri	0.89 ± 0.10	0.98 ± 0.22	0.72 ± 0.24
	C. weissflogii	0.31 ± 0.03	0.34 ± 0.08	0.34 ± 0.02
	P. tricornutum	0.79 ± 0.14[a]	1.84 ± 0.66[ab]	2.18 ± 0.65[b]
	C. fusiformis	0.51 ± 0.11[a]	1.79 ± 0.07[ab]	2.24 ± 1.18[b]
Proteins/lipids	C. muelleri	13.42 ± 2.46[a]	12.57 ± 1.61[a]	5.50 ± 2.60[b]
	C. weissflogii	51.17 ± 11.46[a]	6.80 ± 0.44[b]	6.09 ± 0.26[b]
	P. tricornutum	9.37 ± 1.70	12.83 ± 3.83	7.88 ± 2.25
	C. fusiformis	6.63 ± 0.61[a]	8.73 ± 1.81[a]	231 ± 72[b]
Carbohydrates/lipids	C. muelleri	14.96 ± 3.01[a]	13.21 ± 1.36[a]	7.45 ± 0.96[b]
	C. weissflogii	169 ± 57	36.77 ± 23.97	18.04 ± 1.47
	P. tricornutum	11.92 ± 0.13[a]	7.79 ± 3.67[ab]	3.63 ± 0.05[b]
	C. fusiformis	13.26 ± 1.72[a]	5.01 ± 0.99[a]	57.12 ± 47.48[b]

Data are means of three replicates ± SD. Letters represent significant differences among conditions in the same species (p < 0.05, one-way ANOVA followed by Tukey's *post-hoc* test, results in **Table S3**).

predation pressure, may have influenced both observed paleontological patterns and inferred temporal variation in seawater composition (Falkowski et al., 2004; Zachos et al., 2008; Ratti et al., 2013; Lazarus et al., 2014; Conley et al., 2017; Giordano et al., 2018; Petrucciani et al., 2022). The experiments reported here confirm that whatever other factors inform our understanding of Mesozoic–Cenozoic diatom evolution, declining DSi could have had a direct influence on diatom growth, physiology, and morphogenesis.
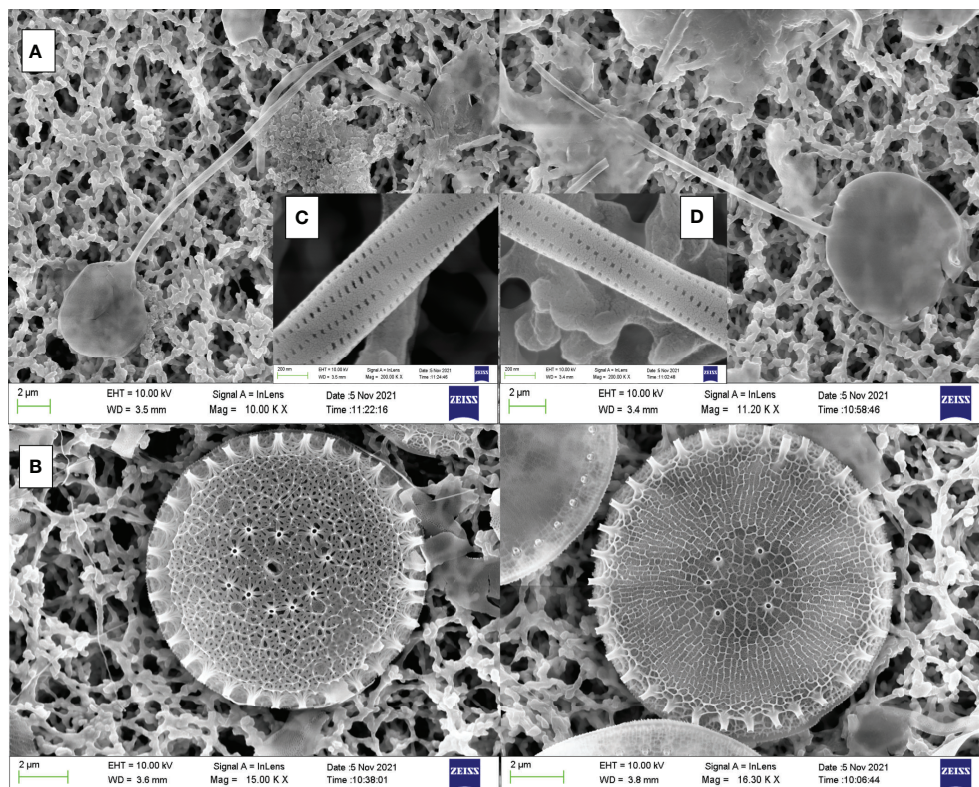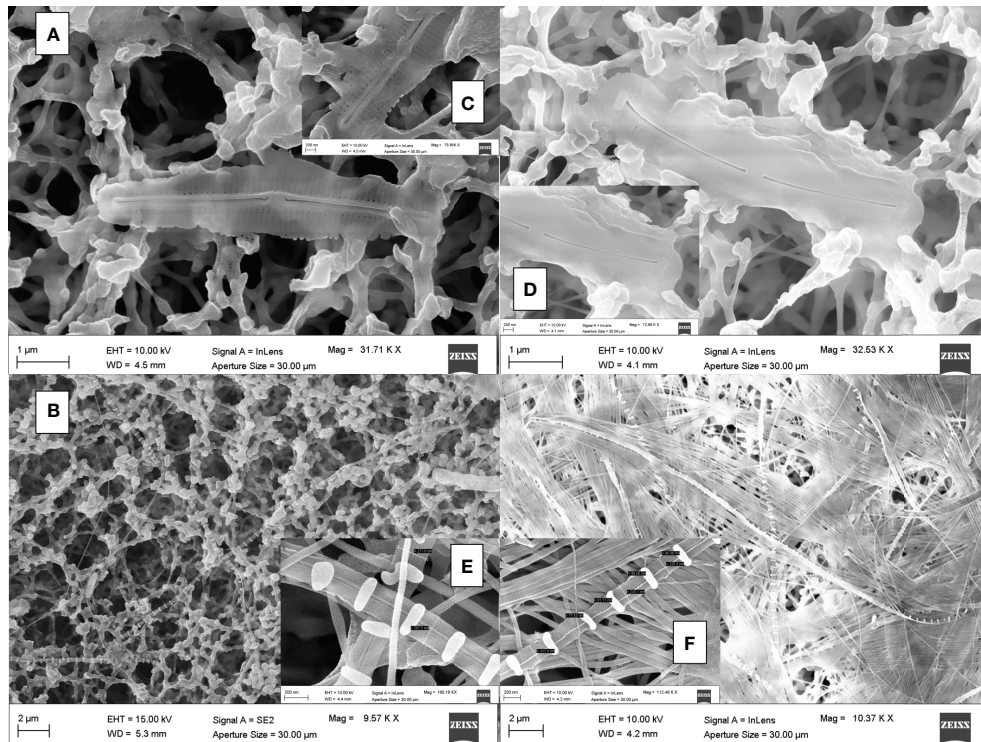

FIGURE 4

SEM images of frustules from *C. muelleri* **(A)** and *C. weissflogii* **(B)** acclimated to 500 μM Si (left images) and 25 μM Si (right images). Details of *C. muelleri* setae at 500 μM Si **(C)** and 25 μM Si **(D)** are shown.

FIGURE 5
SEM images of frustules from *P. tricornutum* **(A)** and *C. fusiformis* **(B)** acclimated to 500 µM Si (left images) and 25 µM Si (right images). Details of *P. tricornutum* and *C. fusiformis* raphe at 500 µM Si (**(C, E)** respectively) and 25 µM Si (**(D, F)** respectively) are shown.

Growth in reconstructed paleoenvironments: facing high [DSi]

Perhaps counterintuitively, our experimental species did not grow better at high DSi concentrations; indeed, just the opposite occurred. All the diatoms in our experiments thrived at the low concentrations of N, Fe, Zn, Mo, and Si characteristic of modern oceans (Table 3 and Figure S1). In modern oceans, regional and seasonal Si limitation (i.e., in the Southern Ocean) is known to downregulate Si uptake and silicification in DSi users, including diatoms (Pinkerton et al., 2021). Nevertheless, diatoms maintain nearly maximal division rates (Olsen and Paasche, 1986). Our data underscore that different species show distinct responses to Si availability. In fact, although growth of the two smaller species, *C. muelleri* and *P. tricornutum*, was significantly lower at the highest DSi concentration (Table 3), the acclimation of *C. muelleri* to 500µM DSi concentration was strongly hampered (Figure S1) as the pennate species reached a stationary phase growth (Figure S1). The drastic reduction in photosynthetic efficiency was consistent with growth limitation (Table 3). It has been suggested that a high silicic acid concentration in the external medium can lead to cytotoxic effects (Marron et al., 2016) through auto-polymerization of intracellular soluble Si which then overaccumulates (Milligan et al., 2004).

Why a high external concentration of DSi should result in a high intracellular Si concentration is unclear. It is known that Si influx makes use of i) energy-dependent transporters for Si uptake (SIT), which have acquired the influx function in response to the scarce availability of Si in oceans, and ii) diffusion (Thamatrakoln et al., 2006; Thamatrakoln and Hildebrand, 2008; Hildebrand et al., 2018). On the other hand, Si efflux is an overlooked and poorly understood process in diatom metabolism. These originally utilized ancestral SITs requiring energy have been hypothesized, as do currently utilized SITs (Martin-Jezequel et al., 2000; Milligan et al., 2004; Thamatrakoln and Hildebrand, 2008; Shrestha and Hildebrand, 2015; Hildebrand et al., 2018). Our data (Table 3 and Figure S1) likely indicate that DSi uptake was not turned off by algal cells; direct damage due to intracellular Si polymerization and/or energy-dependent mechanisms to avoid it (i.e., counterbalancing Si influx with Si efflux) might affect growth as observed for *C. muelleri* and *P. tricornutum*. The effect was observed in less silicified and smaller species characterized by a higher S/V ratio and thus incurring a higher cost to maintain Si homeostasis than bigger cells (Table 3, Figure S1). It is particularly intriguing that in *P. tricornutum*, Fe : Si was the only ratio not modulated by Si availability in the external medium (Table 4). Nevertheless, when DSi was 500 µM, both Si and Fe cell quotas were higher (roughly 17 and 14 times, respectively) than those in modern Si-treated algae

(Table S1). This finding may add nuance to the observation that Fe deficiency leads to enhanced Si content (De La Rocha et al., 2000), suggesting that Fe is strongly involved in Si homeostasis. Further studies are needed to clarify how Fe interacts with Si influx/efflux/biomineralization.

The densely silicified and larger (hence, lower S/V ratio, Table 3 and Figure 1) cells of *C. weissflogii* had a different fate when grown under high DSi conditions (Table 3 and Figure S1). In the presence of higher environmental DSi concentrations, diffusion of silicic acid across membranes is supposed to make a bigger contribution to the Si uptake than it does in lower DSi growth conditions. This could explain why energy is saved and reallocated into *C. weissflogii* growth, assuming that DSi influx through SITs is less relevant and the efflux is not needed due to the high Si requirement for thicker *C. weissflogii* frustules. Only in this species did the photosynthetic efficiency remain unchanged by varying DSi levels (Table 3).

Cell composition in reconstructed paleoenvironments: facing high [DSi]

Cell composition in terms of macromolecular pools varied among treatments and in a shape-dependent manner. At high [DSi], our pre- to early diatom Si treatment cells of pennate diatoms were most costly (in terms of energy investment associated with the observed organic composition; Gerotto et al., 2020) and palatable (Palmucci et al., 2011; Ratti et al., 2013), preferentially allocating fixed C into carbohydrates and proteins (Figure 3, Table 5) as compared to the same species acclimated to modern Si treatment.

Data suggest that over geologic time, DSi availability has affected the overall C allocation pattern of diatoms (in particular pennates) and, therefore, predation pressure *via* its influence on palatability for predators. Thus, DSi decline has favored the evolution of energy-saving, less palatable cells, which are more competitive in intraspecific and interspecific interactions (Petrucciani et al., 2022).

Interestingly, Si availability also affected C isotopic fractionation: when DSi concentration was higher, pennate diatoms increased C fractionation (more negative $\delta^{13}C$) (Figure 2). This could be explained by a change in availability of intracellular inorganic carbon among growth regimes: in fact, a lower contribution of inorganic C mobilized from HCO_3^- to the fixed C in pennates grown in high DSi conditions results in increased discrimination against $^{13}CO_2$ (Korb et al., 1996; Keller and Morel, 1999; Vuorio et al., 2006). This may well reflect to a downregulation in pennates of CCM (Riebesell et al., 2000) in favor of other mandatory energy-dependent mechanisms such as Si deposition and Si efflux under high DSi conditions (Giordano et al., 2005; Giordano et al., 2017). Therefore, lower photosynthetic efficiencies were reported (Table 3). In any event, the correlation between silicon content and C fractionation observed in these species underscores the deep interaction between the two elements as well as between biomineralization

and C fixation (Figure S3). This is somewhat unexpected, since in centric diatoms the uncoupling of silicon compared with carbon and nitrogen metabolisms was reported (Claquin et al., 2002; Suroy et al., 2015). The observed variations in isotopic fractionation also add further nuance to physiological and paleoenvironmental interpretations of organic carbon isotopes in Mesozoic and Cenozoic marine sediments (Hayes et al., 1999).

Greater availability of DSi was associated, as well, with a greater accumulation of Si in both cells (Figure 1, Table S1) and frustules (Figures 4 and 5), as also evident in the literature compilation of Finkel et al (2010). The high Si content was not simply a function of greater cell volume since Si content expressed on a per-volume basis was also higher in the 500μM Si treatment (Figure 1). In addition, a higher Si quota per cell in diatoms is known to be induced by a slower growth rate (Brzezinski et al., 1990; Friedrichs et al., 2013). Both factors (high DSi and low growth rate) were present when *C. muelleri* and *P. tricornutum* showed the highest Si content (Table 3 and Figure S1). The change in Si quota was striking in pennate diatoms (Figure 1 and Table S1), as shown by raphe thickening in *P. tricornutum* frustules (Figures 5A, B). The entire cellular stoichiometry was overturned (Table 4). *C. fusiformis* showed a similar trend, suggesting that the pennate diatoms acclimated to changing growth conditions by modulating Si use efficiency: the higher the available DSi in the environment, the lower the efficiency in its use (Table 4). In contrast, centric diatoms had a homeostatic behavior regarding their elemental stoichiometry: such strategy did not allow growth in *C. muelleri* and limited maximal cell density in *C. weissflogii* (Table 4 and Figure S1).

In conclusion, even with our small sample size, it becomes clear that diatom responses to changing silica bioavailability are commonly individualistic; that is, there may be few parameters for which diatoms universally respond in the same way. The centric and pennate species in our experiments commonly responded in different ways or to different degrees, suggesting that centrics and pennates may show broad and consistent differences in their physiological responses to changing DSi levels.

While we cannot discount climate change and changing preservational selectivity as influences on the observed fossil record of diatoms, the experimental approach used here acclimating algal species to reconstructed paleoenvironments bolsters the case that decreasing [DSi] had an important influence on diatom biomineralization through time. In particular, the observed physiological responses of pennate species may have helped to drive their differential diversification, governing reduced size and silica usage in diatoms as a group.

Data availability statement

The original contributions presented in the study are included in the article/supplementary material. Further inquiries can be directed to the corresponding author.

Author contributions

AP carried out all the experiments and analyzed the data. AHK designed the paleo-reconstructed media and provided a geological perspective to the manuscript. AN conceived and designed the project. AP, AHK, and AN wrote the paper. All authors contributed to the article and approved the submitted version.

Funding

Acknowledgments

Conflict of interest

The authors declare that the research was conducted in the absence of any commercial or financial relationships that could be construed as a potential conflict of interest.

Publisher's note

All claims expressed in this article are solely those of the authors and do not necessarily represent those of their affiliated organizations, or those of the publisher, the editors and the reviewers. Any product that may be evaluated in this article, or claim that may be made by its manufacturer, is not guaranteed or endorsed by the publisher.

Supplementary material

The Supplementary Material for this article can be found online at: https://www.frontiersin.org/articles/10.3389/fmars.2022.924452/full#supplementary-material.

References

Armbrust, E. V. (2009). The life of diatoms in the world's oceans. *Nature* 459, 185–192. doi: 10.1038/nature08057

Benoiston, A. S., Ibarbalz, F. M., Bittner, L., Guidi, L., Jahn, O., Dutkiewicz, S., et al. (2017). The evolution of diatoms and their biogeochemical functions. *Phil. Trans. R. Soc B* 372, 20160397. doi: 10.1098/rstb.2016.0397

Boyle, E. (1998). Pumping iron makes thinner diatoms. *Nature* 393, 733–734. doi: 10.1038/31585

Brzezinski, M., Olson, R., and Chisholm, S. (1990). Silicon availability and cell-cycle progression in marine diatoms. *Mar. Ecol. Prog. Ser.* 67, 83–96. doi: 10.3354/meps067083

Bucciarelli, E., Pondaven, P., and Sarthou, G. (2010). Effects of an iron-light co-limitation on the elemental composition (Si, c, n) of the marine diatoms *Thalassiosira oceanica* and *Ditylum brightwellii*. *Biogeosciences* 7 (2), 657–669. doi: 10.5194/bg-7-657-2010

Cermeño, P., Falkowski, P. G., Romero, O. E., Schaller, M. F., and Vallina, S. M. (2015). Continental erosion and the Cenozoic rise of marine diatoms. *Proc. Natl. Acad. Sci. U.S.A.* 112, 4239–4244. doi: 10.1073/pnas.1412883112

Claquin, P., Martin-Jézéquel, V., Kromkamp, J. C., Veldhuis, M. J. W., and Kraay, G. W. (2002). Uncoupling of silicon compared with carbon and nitrogen metabolisms and the role of the cell cycle in continuous cultures of thalassiosira pseudonana (bacillariophyceae) under light, nitrogen, and phosphorus control. *J. Phycology* 38, 922–930. doi: 10.1046/j.1529-8817.2002.t01-1-01220.x

Cohen, N. R., Ellis, K. A., Lampe, R. H., McNair, H., Twining, B. S., Maldonado, M. T., et al. (2017). Diatom transcriptional and physiological responses to changes in iron bioavailability across ocean provinces. *Front. Mar. Sci.* 4. doi: 10.3389/fmars.2017.00360

Conley, D. J., and Carey, J. C. (2015). Silica cycling over geologic time. *Nat. Geosci* 8, 431–432. doi: 10.1038/ngeo2454

Conley, D. J., Frings, P. J., Fontorbe, G., Clymans, W., Stadmark, J., Hendry, K. R., et al. (2017). Biosilicification drives a decline of dissolved si in the oceans through geologic time. *Front. Mar. Sci.* 4. doi: 10.3389/fmars.2017.00397

De La Rocha, C., Hutchins, D., Brzezinski, M., and Zhang, Y. (2000). Effects of iron and zinc deficiency on elemental composition and silica production by diatoms. *Mar. Ecol. Prog. Ser.* 195, 71–79. doi: 10.3354/meps195071

Domenighini, A., and Giordano, M. (2009). Fourier Transform infrared spectroscopy of microalgae as a novel tool for biodiversity studies, species identification, and the assessment of water quality 1. *J. phycology* 45 (2), 522–531. doi: 10.1111/j.1529-8817.2009.00662.x

Durkin, C. A., Koester, J. A., Bender, S. J., and Armbrust, E. V. (2016). The evolution of silicon transporters in diatoms. *J. phycology* 52, 716–731. doi: 10.1111/jpy.12441

Falkowski, P. G., Katz, M. E., Knoll, A. H., Quigg, A., Raven, J. A., Schofield, O., et al. (2004). The evolution of modern eukaryotic phytoplankton. *Science* 305, 354–360. doi: 10.1126/science.1095964

Fanesi, A., Raven, J. A., and Giordano, M. (2014). Growth rate affects the responses in the green alga *Tretaselmis suecica* to the external perturbation. *Plant Cell Environ.* 37 (2), 512–519. doi: 10.1111/pce.12176

Finkel, Z. V., Katz, M. E., Wright, J. D., Schofield, O. M. E., and Falkowski, P. G. (2005). Climatically driven macroevolutionary patterns in the size of marine diatoms over the Cenozoic. *Proc. Natl. Acad. Sci.* 102, 8927–8932. doi: 10.1073/pnas.0409907102

Finkel, Z. V., and Kotrc, B. (2010). Silica use through time: macroevolutionary change in the morphology of the diatom fustule. *Geomicrobiology J.* 27, 596–608. doi: 10.1080/01490451003702941

Finkel, Z. V., Matheson, K. A., Regan, K. S., and Irwin, A. J. (2010). Genotypic and phenotypic variation in diatom silicification under paleo-oceanographic conditions: Diatom silicification. *Geobiology* 8, 433–445. doi: 10.1111/j.1472-4669.2010.00250.x

Fontorbe, G., Frings, P. J., de la Rocha, C. L., Hendry, K. R., Carstensen, J., and Conley, D. J. (2017). Enrichment of dissolved silica in the deep equatorial pacific during the Eocene-oligocene: Equatorial pacific DSi enrichment. *Paleoceanography* 32, 848–863. doi: 10.1002/2017PA003090

Friedrichs, L., Hörnig, M., Schulze, L., Bertram, A., Jansen, S., and Hamm, C. (2013). Size and biomechanic properties of diatom frustules influence food uptake by copepods. *Mar. Ecol. Prog. Ser.* 481, 41–51. doi: 10.3354/meps10227

Frings, P. J., Clymans, W., Fontorbe, G., de la Rocha, C. L., and Conley, D. J. (2016). The continental Si cycle and its impact on the ocean Si isotope budget. *Chem. Geology* 425, 12–36. doi: 10.1016/j.chemgeo.2016.01.020

Gerotto, C., Norici, A., and Giordano, M. (2020). Toward enhanced fixation of CO2 in aquatic biomass: Focus on microalgae. *Front. Energy Res.* 8. doi: 10.3389/fenrg.2020.00213

Giordano, M., Beardall, J., and Raven, J. A. (2005). CO₂ concentrating mechanisms in algae: mechanisms, environmental modulation, and evolution. *Annu. Rev. Plant Biol.* 56, 99–131. doi: 10.1146/annurev.arplant.56.032604.144052

Giordano, M., Kansiz, M., Heraud, P., Beardall, J., Wood, B., and McNaughton, D. (2001). Fourier Transform infrared spectroscopy as a novel tool to investigate

changes in intracellular macromolecular pools in the marine microalga chaetoceros muellerii (bacillariophyceae). *J. Phycology* 37, 271–279. doi: 10.1046/j.1529-8817.2001.037002271.x

Giordano, M., Norici, A., and Beardall, J. (2017). Impact of inhibitors of amino acid, protein, and RNA synthesis on c allocation in the diatom *Chaetoceros muellerii*: a FTIR approach. *ALGAE* 32, 161–170. doi: 10.4490/algae.2017.32.6.6

Giordano, M., Olivieri, C., Ratti, S., Norici, A., Raven, J. A., and Knoll, A. H. (2018). A tale of two eras: Phytoplankton composition influenced by oceanic paleochemistry. *Geobiology* 16, 498–506. doi: 10.1111/gbi.12290

Girard, V., Saint Martin, S., Buffetaut, E., Saint Martin, J. P., Néraudeau, D., Peyrot, D., et al. (2020). Thai Amber: insights into early diatom history? *Bull. la Société Géologique France* 2020 191 (1), 23. doi: 10.1051/bsgf/2020028

Harper, H. E., and Knoll, A. H. (1975). Silica, diatoms, and Cenozoic radiolarian evolution. *Geol* 3, 175. doi: 10.1130/0091-7613(1975)3<175:SDACRE>2.0.CO;2

Hayes, J. M., Strauss, H., and Kaufman, A. J. (1999). The abundance of ^{13}C in marine organic matter and isotopic fractionation in the global biogeochemical cycle of carbon during the past 800 ma. *Chem. Geology* 161, 103–125. doi: 10.2475/ajs.289.4.436

Hendry, K. R., Marron, A. O., Vincent, F., Conley, D. J., Gehlen, M., Ibarbalz, F. M., et al. (2018). Competition between silicifiers and non-silicifiers in the past and present ocean and its evolutionary impacts. *Front. Mar. Sci.* 5. doi: 10.3389/fmars.2018.00022

Hildebrand, M., Lerch, S. J. L., and Shrestha, R. P. (2018). Understanding diatom cell wall silicification-moving forward. *Front. Mar. Sci.* 5. doi: 10.3389/fmars.2018.00125

Hutchins, D. A., and Bruland, K. W. (1998). Iron-limited diatom growth and Si: N uptake ratios in a coastal upwelling regime. *Nature* 393, 561–564. doi: 10.1038/31203

Keller, K., and Morel, F. (1999). A model of carbon isotopic fractionation and active carbon uptake in phytoplankton. *Mar. Ecol. Prog. Ser.* 182, 295–298. doi: 10.3354/meps182295

Kidder, D. L., and Tomescu, I. (2016). Biogenic chert and the Ordovician silica cycle. *Palaeogeography Palaeoclimatology Palaeoecol.* 458, 29–38. doi: 10.1016/j.palaeo.2015.10.013

Knoll, A. H., and Follows, M. J. (2016). A bottom-up perspective on ecosystem changes in mesozoic oceans. *Proc. R. Soc B.* 283, 20161755. doi: 10.1098/rspb.2016.1755

Korb, R., Raven, J., Johnston, A., and Leftley, J. (1996). Effects of cell size and specific growth rate on stable carbon isotope discrimination by two species of marine diatom. *Mar. Ecol. Prog. Ser.* 143, 283–288. doi: 10.3354/meps143283

Kotrc, B., and Knoll, A. H. (2015). A morphospace of planktonic marine diatoms. i. two views of disparity through time. *Paleobiology* 41, 45–67. doi: 10.1017/pab.2014.4

Lazarus, D., Barron, J., Renaudie, J., Diver, P., and Türke, A. (2014). Cenozoic Planktonic marine diatom diversity and correlation to climate change. *PloS One* 9, e84857. doi: 10.1371/journal.pone.0084857

Lazarus, D. B., Kotrc, B., Wulf, G., and Schmidt, D. N. (2009). Radiolarians decreased silicification as an evolutionary response to reduced Cenozoic ocean silica availability. *Proc. Natl. Acad. Sci.* 106, 9333–9338. doi: 10.1073/pnas.0812979106

Loucaides, S., Van Cappellen, P., Roubeix, V., Moriceau, B., and Ragueneau, O. (2012). Controls on the recycling and preservation of biogenic silica from biomineralization to burial. *Silicon* 4, 7–22. doi: 10.1007/s12633-011-9092-9

Maldonado, M., Carmona, M. C., Uriz, M. J., and Cruzado, A. (1999). Decline in mesozoic reef-building sponges explained by silicon limitation. *Nature* 401, 785–788. doi: 10.1038/44560

Maliva, R. G., Knoll, A. H., and Siever, R. (1989). Secular change in chert distribution: a reflection of evolving biological participation in the silica cycle. *PALAIOS* 4, 519. doi: 10.2307/3514743

Malviya, S., Scalco, E., Audic, S., Vincent, F., Veluchamy, A., Poulain, J., et al. (2016). Insights into global diatom distribution and diversity in the world's ocean. *Proc. Natl. Acad. Sci. U.S.A.* 113, E1516–E1525. doi: 10.1073/pnas.1509523113

Marron, A. O., Ratcliffe, S., Wheeler, G. L., Goldstein, R. E., King, N., Not, F., et al. (2016). The evolution of silicon transport in eukaryotes. *Mol. Biol. Evol.* 33, 3226–3248. doi: 10.1093/molbev/msw209

Martin-Jezequel, V., Hildebrand, M., and Brzezinski, M. A. (2000). Silicon metabolism in diatoms: implications for growth. *J. Phycol* 36, 821–840. doi: 10.1046/j.1529-8817.2000.00019.x

Medlin, L. K. (2015). A timescale for diatom evolution based on four molecular markers: reassessment of ghost lineages and major steps defining diatom evolution. *Vie Milieu* 65 (4), 821–840.

Meyerink, S., Ellwood, M. J., Maher, W. A., and Strzepek, R. (2017). Iron availability influences silicon isotope fractionation in two southern ocean diatoms

(*Proboscia inermis* and *Eucampia antarctica*) and a coastal diatom (*Thalassiosira pseudonana*). *Front. Mar. Sci.* 4, 217. doi: 10.3389/fmars.2017.00217

Milligan, A. J., Varela, D. E., Brzezinski, M. A., and Morel, F. M. M. (2004). Dynamics of silicon metabolism and silicon isotopic discrimination in a marine diatoma as a function of pCO $_2$. *Limnol. Oceanogr.* 49, 322–329. doi: 10.4319/lo.2004.49.2.0322

Misra, A. N., Misra, M., and Singh, R. (2012). Chlorophyll fluorescence in plant biology. *Biophysics.* 49, 322–329. doi: 10.4319/lo.2004.49.2.0322

Monod, J. (1949). The growth of bacterial cultures. *Annu. Rev. Microbiol.* 3, 371–394. doi: 10.1146/annurev.mi.03.100149.002103

Mosseri, J., Quéguiner, B., Armand, L., and Cornet-Barthaux, V. (2008). Impact of iron on silicon utilization by diatoms in the southern ocean: A case study of Si/N cycle decoupling in a naturally iron-enriched area. *Deep Sea Res. Part II: Topical Stud. Oceanography* 55, 801–819. doi: 10.1016/j.dsr2.2007.12.003

Olsen, S., and Paasche, E. (1986). Variable kinetics of silicon-limited growth in *Thalassiosira pseudonana* (Bacillariophyceae) in response to changed chemical composition of the growth medium. *Br. Phycological J.* 21, 183–190. doi: 10.1080/00071618600650211

Palmucci, M., Ratti, S., and Giordano, M. (2011). Ecological and evolutionary implications of carbon allocation in marine phytoplankton as a function of nitrogen availability: a fourier transform infrared spectroscopy approach1: c allocation as a function of n availability. *J. Phycology* 47, 313–323. doi: 10.1111/j.1529-8817.2011.00963.x

Panagiotopoulos, C., Goutx, M., Suroy, M., and Moriceau, B. (2020). Phosphorus limitation affects the molecular composition of *Thalassiosira weissflogii* leading to increased biogenic silica dissolution and high degradation rates of cellular carbohydrates. *Organic Geochemistry* 148, 104068. doi: 10.1016/j.orggeochem.2020.104068

Peterson, G. L. (1977). A simplification of the protein assay method of lowry et al. which is more generally applicable. *Analytical Biochem.* 83 2, 346–356. doi: 10.1016/0003-2697(77)90043-4

Petrucciani, A., Chaerle, P., and Norici, A. (2022). Diatoms versus copepods: could frustule traits have a role in avoiding predation? *Front. Mar. Sci.* 8. doi: 10.3389/fmars.2021.804960

Pinkerton, M. H., Boyd, P. W., Deppeler, S., Hayward, A., Höfer, J., and Moreau, S. (2021). Evidence for the impact of climate change on primary producers in the southern ocean. *Front. Ecol. Evol.* 9, 592027. doi: 10.3389/fevo.2021.592027

Rabosky, D. L., and Sorhannus, U. (2009). Diversity dynamics of marine planktonic diatoms across the Cenozoic. *Nature* 457, 183–186. doi: 10.1038/nature07435

Racki, G., and Cordey, F. (2000). Radiolarian palaeoecology and radiolarites: is the present the key to the past? *Earth-Science Rev.* 52, 83–120. doi: 10.1016/S0012-8252(00)00024-6

Ragueneau, O., Schultes, S., Bidle, K., Claquin, P., and Moriceau, B. (2006). Si And c interactions in the world ocean: Importance of ecological processes and implications for the role of diatoms in the biological pump: Si and c interactions in the ocean. *Global Biogeochem. Cycles* 20, n/a–n/a. doi: 10.1029/2006GB002688

Ratti, S., Knoll, A. H., and Giordano, M. (2011). Did sulfate availability facilitate the evolutionary expansion of chlorophyll a+c phytoplankton in the oceans? sulfate and evolution of chlorophyll a+c phytoplankton. *Geobiology* 9, 301–312. doi: 10.1111/j.1472-4669.2011.00284.x

Ratti, S., Knoll, A. H., and Giordano, M. (2013). Grazers and phytoplankton growth in the oceans: an experimental and evolutionary perspective. *PloS One* 8, e77349. doi: 10.1371/journal.pone.0077349

Reimann, B. E. F., Lewin, J. C., and Volcani, B. E. (1965). Studies on the biochemistry and fine structure of silica shell formation in diatoms: I. the structure of the cell wall of *Cylindrotheca fusiformis*. *J. Cell Biol.* 24, 39–55. doi: 10.1083/jcb.24.1.39

Reinke, D. C. (1984). Ultrastructure of *Chaetoceros muelleri* (bacillariophyceae): auxospore, resting spore and vegetative cell morphology. *J. Phycology* 20, 153–155. doi: 10.1111/j.0022-3646.1984.00153.x

Renaudie, J. (2016). Quantifying the Cenozoic marine diatom deposition history: links to the c and Si cycles. *Biogeosciences* 13, 6003–6014. doi: 10.5194/bg-13-6003

Riebesell, U., Burkhardt, S., Dauelsberg, A., and Kroon, B. (2000). Carbon isotope fractionation by a marine diatom: dependence on the growth-rate-limiting resource. *Mar. Ecol. Prog. Ser.* 193, 295–303. doi: 10.3354/meps193295

Ritchie, R. J. (2006). Consistent sets of spectrophotometric chlorophyll equation for acetone, methanol, and ethanol solvents. *Photosynthesis Res.* 89, 27–41. doi: 10.1007/s11100-006-9065-9

Shrestha, R. P., and Hildebrand, M. (2015). Evidence for a regulatory role of diatom silicon transporters in cellular silicon responses. *Eukaryot Cell* 14, 29–40. doi: 10.1128/EC.00209-14

Siever, R. (1992). The silica cycle in the precambrian. *Geochimica Cosmochimica Acta* 56, 3265–3272. doi: 10.1016/0016-7037(92)90303-Z

Suroy, M., Panagiotopoulos, C., Boutorh, J., Goutx, M., and Moriceau, B. (2015). Degradation of diatom carbohydrates: A case study with n- and Si-stressed thalassiosira weissflogii. *J. Exp. Mar. Biol. Ecol.* 470, 1–11. doi: 10.1016/j.jembe.2015.04.018

Sutton, J. N., André, L., Cardinal, D., Conley, D. J., de Souza, G. F., Dean, J., et al. (2018). A review of the stable isotope bio-geochemistry of the global silicon cycle and its associated trace elements. *Front. Earth Sci.* 5, 112. doi: 10.3389/feart.2017.00112

Takeda, S. (1998). Influence of iron availability on nutrient consumption ratio of diatoms in oceanic waters. *Nature* 393, 774–777. doi: 10.1038/31674

Thamatrakoln, K., Alverson, A. J., and Hildebrand, M. (2006). Comparative sequence analysis of diatom silicon transporters: toward a mechanistic model of silicon transport. *J. Phycology* 42, 822–834. doi: 10.1111/j.1529-8817.2006.00233.x

Thamatrakoln, K., and Hildebrand, M. (2008). Silicon uptake in diatoms revisited: a model for saturable and nonsaturable uptake kinetics and the role of silicon transporters. *Plant Physiol.* 146, 1397–1407. doi: 10.1104/pp.107.107094

Tréguer, P., Bowler, C., Moriceau, B., Dutkiewicz, S., Gehlen, M., Aumont, O., et al. (2018). Influence of diatom diversity on the ocean biological carbon pump. *Nat. Geosci* 11, 27–37. doi: 10.1038/s41561-017-0028-x

Tréguer, P. J., Sutton, J. N., Brzezinski, M., Charette, M. A., Devries, T., Dutkiewicz, S., et al. (2021). Reviews and syntheses: The biogeochemical cycle of silicon in the modern ocean. *Biogeosciences* 18, 1269–1289. doi: 10.5194/bg-18-1269-2021

Trower, E. J., Strauss, J. V., Sperling, E. A., and Fischer, W. W. (2021). Isotopic analyses of Ordovician–Silurian siliceous skeletons indicate silica-depleted Palaeozoic oceans. *Geobiology* 19, 460–472. doi: 10.1111/gbi.12449

Vallina, S. M., Follows, M. J., Dutkiewicz, S., Montoya, J. M., Cermeno, P., and Loreau, M. (2014). Global relationship between phytoplankton diversity and productivity in the ocean. *Nat. Commun.* 5, 4299. doi: 10.1038/ncomms5299

Vincent, F., and Bowler, C. (2020). Diatoms are selective segregators in global ocean planktonic communities. *mSystems* 5 (1), e00444–19. doi: 10.1128/mSystems.00444-19

Vuorio, K., Meili, M., and Sarvala, J. (2006). Taxon-specific variation in the stable isotopic signatures (δ^{13}C and δ^{15}N) of lake phytoplankton. *Freshw. Biol.* 51, 807–822. doi: 10.1111/j.1365-2427.2006.01529.x

Wellburn, A. R. (1994). The spectral determination of chlorophylls a and b, as well as total carotenoids, using various solvents with spectrophotometers of different resolution. *J. Plant Physiol.* 1443, 307–313. doi: 10.1016/S0176-1617(11)81192-2

Westacott, S., Planavsky, N. J., Zhao, M. Y., and Hull, P. M. (2021). Revisiting the sedimentary record of the rise of diatoms. *PNAS* 118 (27), e2103517118. doi: 10.1073/pnas.2103517118

Zachos, J. C., Dickens, G. R., and Zeebe, R. E. (2008). An early Cenozoic perspective on greenhouse warming and carbon-cycle dynamics. *Nature* 451, 279–283. doi: 10.1038/nature06588